

# Divergent behavior of hydrothermal plumes in fresh versus salty icy ocean worlds

Suyash Bire<sup>1</sup>, Tushal Mittal<sup>1</sup>, Wanying Kang<sup>1</sup>, Ali Ramadhan<sup>1</sup>, Philip J. Tuckman<sup>1</sup>, Christopher R. German<sup>2</sup>, Andreas Thurnherr<sup>3</sup>, John Marshall<sup>1</sup>

<sup>1</sup>Earth, Atmospheric, and Planetary Sciences, Massachusetts Institute of Technology, Cambridge, MA 02139 US

<sup>2</sup>Woods Hole Oceanographic Institution, 266 Woods Hole Road, Woods Hole, MA 02543-1050

<sup>3</sup>Lamont-Doherty Earth Observatory, 61 Route 9W, Palisades, NY 10964

## Key Points:

- Salty oceans near the freezing point develop buoyant plumes which rise in the water column when energised by localised hydrothermal vents.
- Buoyant plumes become diluted by turbulence and baroclinic instability as they rise upwards.
- Fresh oceans develop bottom-hugging currents when heated near the freezing point, because of the contraction of fluid parcels on warming.

---

Corresponding author: Suyash Bire, [bire@mit.edu](mailto:bire@mit.edu)

**Abstract**

Water parcels close to their freezing point contract and become heavy on warming if they are sufficiently fresh, but expand and become buoyant when salty. We explore the resulting divergent behavior of hydrothermal plumes in fresh versus salty icy ocean worlds, with particular emphasis on Enceladus and Europa. Salty oceans develop buoyant plumes which rise upwards in the water column when energized by localised hydrothermal vents. Fresh oceans, instead, develop bottom-hugging gravity currents when heated near the freezing point, because of the anomalous contraction of fluid parcels on warming. The contrasting dynamics are highlighted and the implications discussed.

**Plain Language Summary**

Oceans on icy moons such as Enceladus and Europa may potentially have many of the conditions required for life. The possible existence of hydrothermal vents on the ocean floors of these moons are prime candidates as sources of biological activity. Here we explore the conditions in which heating at bottom vents might lead to convection that could carry biomarkers from the bottom of the ocean up to the ice. We argue that if the background salinity is low, heating close to the freezing point of water leads to dense, bottom-hugging density currents. If the water is salty, however, upward-reaching plummy convection can result.

**1 Introduction**

Since the Cassini mission, Enceladus has become a prominent astrobiological target with potentially many of the conditions required for habitability (Cable et al., 2021; Glass et al., 2022; Hand et al., 2020). Enceladus is an archetype of a broader class of icy ocean worlds, a number of which may also be habitable (Nimmo & Pappalardo, 2016; Vance et al., 2018). Early observations of geological features on its ice shell led to speculations on the presence of an active subsurface ocean (Nimmo & Pappalardo, 2016). The subsequent discovery of plumes emanating from the south pole of Enceladus boosted the idea that Enceladus might possess a significant subsurface ocean (Porco et al., 2006; Hansen et al., 2006). Observations and modeling studies of exaggerated libration on Enceladus, along with gravity-topography analysis, have all but confirmed the presence of a global subsurface ocean with an average thickness of 35 - 45 km (e.g. Thomas et al., 2016; Čadež et al., 2016; Van Hoolst et al., 2016; Beuthe et al., 2016; Hemingway & Mittal, 2019). Additionally, studies of the composition of the plumes have indicated the presence of silica nanoparticles (Hsu et al., 2015; Sekine et al., 2015), hydrogen (Waite et al., 2017), as well as salts and organic compounds (Postberg et al., 2018; Fifer et al., 2022). The actual salinity of the ocean is still a matter of debate.

Such observations are suggestive of active hydrothermal activity, with Enceladus's rocky core providing the thermochemical energy for potential life at/beneath the seafloor (Choblet et al., 2021). Furthermore, Choblet et al. (2017) show that if the porous rocky core (20-30 % porosity e.g. Hemingway and Mittal (2019)) is highly dissipative, core-scale porous media convection might focus hydrothermal activity at the poles. Rovira-Navarro et al. (2022) find qualitatively similar results for Enceladus's core using a poroviscoelastic rheology. However, viscous dissipation in the core can drive geological activity only if it has a low rigidity and viscosity. Choblet et al. (2017) also suggest, using scaling results from Goodman and Lenferink (2012), that hydrothermal heat localization could be sufficient to power hydrothermal plumes all the way up to the ice-ocean interface on a timescale of months.

In contrast to the aforementioned observational/porous flow modeling for Enceladus, most studies of convection or hydrothermal plume dynamics on icy moons have focused on Europa and/or have prescribed high seafloor heat fluxes (Goodman et al., 2004;

65 Goodman & Lenferink, 2012; Soderlund et al., 2013; Ashkenazy & Tziperman, 2021; Bire  
 66 et al., 2022). For example, Goodman et al. (2004) conducted laboratory experiments and  
 67 derived scaling laws to predict the timescale over which plumes from the bottom of Eu-  
 68 ropa’s ocean would reach the surface. Additionally, they show that any given plume’s  
 69 life cycle would involve an initial transient stage when the effects of planetary rotation  
 70 are not felt, an intermediate stage where the plume rises to the surface in a cylindrical  
 71 column, and a final stage in which the plume becomes baroclinically unstable and sheds  
 72 secondary vortices. The main outcome was that predictions could be made about the  
 73 efficiency of heat transfer from the sea floor to the base of the ice shell. Goodman and  
 74 Lenferink (2012) tested these findings through numerical simulations. One such simu-  
 75 lation is repeated here. Both of these studies suggest that plumes might transport about  
 76  $0.1$  to  $10 \text{ W m}^{-2}$  from the seafloor to the base of the ice shell and span diameters of  $O(10 \text{ km})$ .  
 77 Note that these models used heat fluxes which are significantly larger than that which  
 78 is nominally expected on Europa and Enceladus (Choblet et al., 2017).

79 Based on these findings, as well as models of hydrothermal circulation in icy ocean  
 80 worlds (e.g., Choblet et al. (2017) and Steel et al. (2017) for Enceladus, Běhounková et  
 81 al. (2021) for Europa) it has been assumed that for an unstratified/weakly stratified ocean,  
 82 hydrothermal plumes might traverse the ocean almost vertically on timescales of days-  
 83 months. This paradigm provided the framework for the interpretation of geochemical  
 84 measurements of plume particles on Enceladus and for the spectroscopy of surface ma-  
 85 terial on Europa/other icy ocean worlds. For example, Hsu et al. (2015) observe silica  
 86 nanoparticles in plume ejecta from the south pole of Enceladus. Hsu et al. (2015) and  
 87 Sekine et al. (2015) posited that these particles originated from hydrothermal reactions  
 88 in the rocky core and transited across the Enceladean ocean of thickness of  $O(10 \text{ km})$  in  
 89 a matter of days-weeks. In order to match observational constraints on particle size, these  
 90 studies also constrain the salinity of the Enceladean ocean, suggesting it to be less than  
 91 4% (or  $40 \text{ g kg}^{-1}$  or  $40 \text{ psu}$ ). In addition, this paradigm of fast hydrothermal plume trans-  
 92 port is also the basis of models explaining various surface geological features or surface  
 93 shell thickness variations on icy satellites (e.g. Čadek et al., 2019; Kvorcka et al., 2018)  
 94 using model results from solid core processes. Finally, an efficient transport from seafloor  
 95 to ice shell (and potentially to the surface through jets or other cryovolcanism) is a key  
 96 motivator for future space missions to these bodies seeking extraterrestrial life, especially  
 97 mission concepts arguing for landing on the ice shell and scooping surface material de-  
 98 posited by the plumes (Choblet et al., 2021; MacKenzie et al., 2022). Typically, it has  
 99 been assumed that, in analogy with deep sea hydrothermal vents on Earth, the seafloor  
 100 on icy ocean worlds is likely the most habitable environment on such bodies.

101 To the best of our understanding, previous studies have yet to focus on one key geo-  
 102 physical characteristic of hydrothermal plume dynamics: the influence of ocean salinity  
 103 and the equation of state (EOS) of water near the freezing point of water. Previous work  
 104 has analyzed the role of salinity on the large scale circulation of icy ocean worlds and  
 105 shown it to be a key parameter affecting the circulation (Kang et al., 2022; Zeng & Jansen,  
 106 2021). As argued by Kang et al. (2022), the most likely salinity for icy ocean worlds with  
 107 shell thickness variation typical of Enceladus is of intermediate value (that is less than  
 108  $20 \text{ psu}$  ( $\text{g/kg}$ ), see later summary). However, most previous work assumes larger ocean  
 109 salinities, more typical of Earth’s ocean. In this case seawater heated near its freezing  
 110 point becomes lighter than the surroundings and hence rises. In contrast, at lower salin-  
 111 ities, heating of water close to freezing temperatures, actually makes water denser, due  
 112 to the anomalous expansion of near-freezing water (Ede, 1956; Ivanov & Nikolov, 2020).  
 113 In this case, convective plumes driven by core hydrothermal activity are unlikely to di-  
 114 rectly reach the surface.

115 The purpose of this study is to directly address the role of salinity in shaping the  
 116 response of the ocean to hydrothermal heat sources in a parameter space of relevance  
 117 to icy moons. In section 2, we explore the EOS and the effect of salinity and pressure

118 on the thermal expansion coefficient of seawater. Sections 4 and 5 contrast the behav-  
 119 ior of hydrothermal plumes in the cases where the thermal expansion coefficient is pos-  
 120 itive and negative, respectively. Section 6 discusses the implications of our study for var-  
 121 ious icy moons. The numerical simulations designed to study hydrothermal plume dy-  
 122 namics in a nominally Enceladus-like icy moon are described in the supporting informa-  
 123 tion.

## 124 **2 Thermal expansion coefficient of water**

125 One of the key variables that determines the dynamics of hydrothermal plumes is  
 126 the thermal expansion coefficient of water since this controls the buoyancy of fluid parcels  
 127 upon heating. The thermal expansion coefficient of water depends on, amongst other things,  
 128 the amount and type of dissolved solute. Early estimates of the salinity of Enceladus’  
 129 ocean are based on assumptions of thermodynamic equilibrium. Considering a range of  
 130 hydrothermal and freezing conditions for chondritic compositions, an ocean in equilib-  
 131 rium with the rocky core will have a present day salinity of between 2-20 psu (Zolotov,  
 132 2007; Zolotov & Postberg, 2014; Glein et al., 2018a). However, at least  $\sim 17$  psu may  
 133 be required to keep the geysers’ liquid-gas interface convectively active ensuring that  
 134 they do not freeze up (Ingersoll & Nakajima, 2016). Sodium-enriched samples taken by  
 135 Cassini from south pole sprays have a salinity of 5-20 psu. This can be considered a lower  
 136 bound since the interaction of cold water vapor sprays with their environment may lower  
 137 the salinity of droplets through condensation (Postberg et al., 2009). There is consid-  
 138 erable uncertainty, however, since fractional crystallization and disequilibrium chemistry  
 139 may partition components in such a way that geyser particles are not directly represen-  
 140 tative of the underlying ocean (Fox-Powell & Cousins, 2021). Furthermore, if particles  
 141 originate from a hydrothermal vent, composition can deviate far from that of the over-  
 142 all ocean (Glein et al., 2018a; Fifer et al., 2022). It is of note that the size of silica nano-  
 143 particles carried along in the sprays has also been used to estimate ocean salinity. As-  
 144 suming an intermediate value of pH and a short transport timescale induced by hydrother-  
 145 mal activity, a salinity  $< 40$  psu is obtained (Hsu et al., 2015). In a separate line of ar-  
 146 gument, oceans with too much or too little salt may have a strong ice pump effect, lead-  
 147 ing to the erosion of ice thickness gradients (Kang et al., 2022). Europa’s ocean salin-  
 148 ity is even more poorly constrained. The amplitude of the magnetic induction signal sug-  
 149 gests a rather salty ( $> 50$  psu), deep ocean. However, significant degeneracy exists in  
 150 the retrieval process (Hand & Chyba, 2007) and there is uncertainty about the effect of  
 151 accreted volatiles ( $\text{CO}_2$ ,  $\text{NH}_3$ ) on ocean conductivity.

152 The specific chemical composition of the plumes erupting from the south pole of  
 153 Enceladus’ ice shell is also an ongoing field of study (Glein et al., 2018b; Khawaja et al.,  
 154 2019; Fifer et al., 2022; Postberg et al., 2022). Sodium chloride inferred from plume mea-  
 155 surements yields information about the salinity of the ocean on Enceladus (Postberg et  
 156 al., 2009; Glein et al., 2018b). Spectroscopy of the plumes has also indicated the pres-  
 157 ence of ammonia Waite et al. (2017), along with other volatile species. The composition  
 158 of Europa’s ocean is similarly uncertain. Trumbo et al. (2019) report evidence for sodium  
 159 chloride on Europa’s ice crust. Moreover, modeling studies of composition of Europa’s  
 160 ocean suggest that it might be enriched in metallic salts such as magnesium sulphate (Vance  
 161 et al., 2018). Given the distinct initial state and evolutionary history of icy moons, the  
 162 composition of seawater therein could be very distinct from that on earth: the terres-  
 163 trial EOS may not be relevant. Given these possibilities, we now briefly explore the range  
 164 of likely thermal expansion coefficients of water under varying temperatures, pressures,  
 165 and compositions.

166 We first contrast the thermal expansion coefficient of the ocean on Enceladus (fig. 1a)  
 167 with that of Europa (fig. 1b), assuming that an EOS for NaCl dominated water such as  
 168 that on Earth’s ocean (TEOS-10) is appropriate (Millero et al., 2008; Roquet et al., 2015).  
 169 Similarly, in panels c and d we also plot the likely variation of the thermal expansion

170 coefficient on Enceladus and Europa assuming a magnesium sulphate solute using the  
 171 *PlanetProfile* algorithm (Vance et al., 2014). Panel e shows the effect of ammonia on ther-  
 172 mal expansion coefficient on Enceladus.

173 The first pattern to note in all panels is that the thermal expansion coefficient at  
 174 any given temperature and pressure increases with the concentration of salt. The pres-  
 175 ence of ionic compounds in water disrupts its tendency to form hydrogen bonds and causes  
 176 it to expand on heating. Thus, at high concentrations of salts, the thermal expansion  
 177 coefficient of ocean water is always positive. However, at low salt concentrations, we do  
 178 see negative values of  $\alpha$  between temperatures of  $-2$  to  $4^\circ\text{C}$  in panels a, c, and e. Thus,  
 179 fresher oceans result in anomalous behavior in which water close to freezing becomes denser  
 180 upon heating.

181 A second pattern can be seen in fig. 1: panels b and d show that negative values  
 182 of thermal expansion coefficient are only attained at low values of pressure on Europa.  
 183 This behavior results from non-linearities in the equation of state and especially their  
 184 sensitivity to pressure. Since Europa’s gravity is about 10 times stronger than that of  
 185 Enceladus, pressure increases more rapidly with depth on Europa. Assuming ice shell  
 186 thickness on Enceladus and Europa to be 30 km and 10 km, respectively, the hydrostatic  
 187 pressure at a depth of 5 km from the base of the ice shell on Enceladus is 10 bar while  
 188 that on Europa is 150 bar. This difference becomes larger the deeper we go. Therefore,  
 189 in panels b and d, we see that the high pressures at deeper levels in Europa’s ocean sup-  
 190 press anomalous contraction of water under warming.

191 A key conclusion of our EOS survey is that for high salinity Europa-like oceans,  
 192 the effect of salinity is not likely to suppress buoyant, plummy dynamics triggered by bot-  
 193 tom heating. This is true regardless of whether the ocean is dominated by chloride or  
 194 sulfate salts or high ammonia concentrations. On the other hand, in the case of Ence-  
 195 ladus, typical values of salinity estimated from previous studies (Hsu et al., 2015; Kang  
 196 et al., 2022) can place it in the region of negative alpha. While large concentrations of  
 197 ammonia lead to a positive thermal expansion coefficient, small amounts can lead to a  
 198 negative limit for alpha. This is especially important for Enceladus because best current  
 199 estimates of ammonia concentrations there are  $4 - 13 \text{ g kg}^{-1}$  (assuming seawater com-  
 200 position is the direct volume mixing gas abundance ratios in the plume) (Waite et al.,  
 201 2017) and  $0.1 - 2 \text{ g kg}^{-1}$  when accounting for fractionation of gas plume composition due  
 202 to water vapor condensation and gas exsolution (Fifer et al., 2022). At such concentra-  
 203 tions, especially when accounting for gas fractionation, Enceladus’s ocean could indeed  
 204 be in the negative alpha regime.

### 205 **3 Numerical explorations of hydrothermal plumes on fresh versus salty** 206 **icy ocean worlds**

207 We explore by numerical experimentation how the anomalous contraction of water  
 208 warmed near its freezing point impacts the dynamics of hydrothermal plumes. We  
 209 use *Oceananigans.jl*, a state-of-the-art ocean general circulation model written in Julia  
 210 to run fast on graphical processing units (Ramadhan et al., 2020), configured for study  
 211 of hydrothermal plumes run at high-resolution. The domain stretches from 0 to  $L$  in both  
 212 zonal ( $x$ ) and meridional ( $y$ ) directions and from  $z = -H$  to  $z = 0$  in the vertical di-  
 213 rection as shown in fig. 2.  $L$  and  $H$  are set to 10 km and 40 km, respectively, in our two  
 214 experiments for Enceladus-like parameters. The grid is rectilinear with a spacing of 40 m  
 215 in the horizontal and 80 m in the vertical direction. For our experiment with Europa-  
 216 like parameters,  $L$  is extended to 40 km and the horizontal grid spacing is set to 80 m.  
 217 These values for the domain size, and consequently the grid spacing, are chosen based  
 218 on the horizontal scale of the plumes. The periodic nature of the domain means that if  
 219 the domain is too small the plumes self-interact even before they are fully developed. The

220 results in this study are not sensitive to the choice of these parameters as long as the hor-  
221 zontal domain size is wide enough to represent a fully evolved plume.

222 The rotation rate is  $\Omega = 5.3 \times 10^{-5} \text{ s}^{-1}$ , acceleration due to gravity is  $g = 0.1 \text{ m s}^{-2}$ ,  
223 and specific heat capacity is  $C_P = 4000 \text{ J kg}^{-1} \text{ K}^{-1}$ : all values are suitable for Ence-  
224 ladus (Soderlund, 2019). The horizontal and vertical Laplacian diffusivity is  $1.25 \times 10^{-3} \text{ m}^2 \text{ s}^{-1}$   
225 and  $5 \times 10^{-3} \text{ m}^2 \text{ s}^{-1}$ , respectively. The values are chosen such that they ensure numer-  
226 ical stability as well as preserve baroclinic turbulence important for our study. The Prandtl  
227 number is 1.

228 To illustrate the importance of different salinities, we perform two simulations with  
229 salinities of 15 psu and 35 psu which imply a different sign of thermal expansion coef-  
230 ficient. At the bottom,  $z = -H$ , a patch of heating is prescribed thus:

$$Q = Q_0 \exp \left[ -\frac{(x - x_0)^2 + (y - y_0)^2}{2\sigma^2} \right], \quad (1)$$

231 where  $x_0 = y_0 = L/2$  is at the center of the domain and  $\sigma = l/\sqrt{2\pi}$  controls the width  
232 of the heating patch. For our simulations we set  $l$  to 1000 m and  $Q_0$  to  $100 \text{ W m}^{-2}$ . The  
233 choice of  $l$  and  $Q_0$  is informed by the predicted seafloor heat flux and its localization.  
234 The choice of these parameters does not affect the overall conclusions of this study. With  
235 the values we have chosen the total heat flux entering the domain is

$$E = \int \int Q \, dx \, dy = Q_0 l^2, \quad (2)$$

236 which is  $10^8 \text{ W} = 0.1 \text{ GW}$ . If averaged over the entire cross section we obtain  $1 \text{ W m}^{-2}$ .  
237 This value is  $\sim 10$ - $20$  times that suggested by Choblet et al. (2017) which means that  
238 we are applying more heat localization than suggested by them. Applying a lower heat  
239 flux in line with what they suggested does not change the findings of this study. The heat  
240 flux is applied as a temperature flux.

241 We employ the 55 term polynomial approximation to the TEOS-10 proposed by  
242 Roquet et al. (2015). The pressure used in the expressions is scaled by the ratio of Ence-  
243 ladus's gravity to that of the Earth. In the case of a linear equation of state, we can write  
244 the buoyancy flux as,

$$B = \alpha g \frac{Q}{\rho_0 C_P}. \quad (3)$$

245 Note that the buoyancy flux changes sign based on the sign of  $\alpha$ , that is, positive  $\alpha$  pro-  
246 duces buoyant water that tends to rise, while a negative  $\alpha$  produces dense water that  
247 spreads along the bottom.

#### 248 4 Buoyant plumes in saline oceans

249 Fig. 3 shows typical characteristics of a plume originating from a bottom-heated  
250 patch in a salty ocean in which  $S = 35$  psu. The temperature and particles released in  
251 to the flow, as shown in panels b, c, j, and k, indicate that the influence of the bottom  
252 heating patch is to create plumes which rise to a height of roughly 10 km from the seafloor  
253 after 400 rotation periods or so. Based on previous studies one could imagine that wa-  
254 ter just above the heating patch would become more buoyant, even after entraining am-  
255 bient water, and rise upward toward the surface. However, the plan views of horizon-  
256 tal and vertical currents and temperatures shown in panels d to i, reveal that swirling  
257 currents and eddies are created which also sweep warm fluid laterally, not just vertically,  
258 away from the heating source. It is for this reason that our plumes do not reach all the  
259 way up to the surface even after integrating for hundreds of rotation periods.

260 Under the influence of rotation, some of the vertical plume velocity attained by a  
261 buoyant water parcel is converted into horizontal motion thus inhibiting convection through

**Table 1.** Expected parameters for icy moons (Soderlund, 2019) and those used in our simulations are shown in this table. Acceleration due to gravity is  $g$ , thermal expansion coefficient is  $\alpha$ , rotation rate of the moon is  $\Omega$ , depth of the ocean is  $H$ , and heat flux emanating from the patch area is  $Q_0$ . The total heat entering the domain,  $E$ , is calculated using equation (2), the buoyancy flux,  $F$ , is calculated using (5), the rotational length scale,  $l_{rot}$ , and Rossby number,  $Ro^*$ , are calculated using equations (6) and (4), respectively. \*Note that heat flux at the bottom of Europa is not well constrained. We use a value of  $10 \text{ W m}^{-2}$  but it could range from 1 to  $100 \text{ W m}^{-2}$  (Běhounková et al., 2021).

	$g$ $\text{m s}^{-2}$	$\alpha$ $(10^{-4} \text{ K}^{-1})$	$\Omega$ $(10^{-5} \text{ s}^{-1})$	$L$ (km)	$H$ (km)	$Q_0$ $(\text{W m}^{-2})$	$E$ (GW)	$F$ $(10^{-5} \text{ m}^4 \text{ s}^{-3})$	$l_{rot}$ (m)	$Ro^*$ $(10^{-3})$	Salinity (psu)
Icy moons											
	Europa	2.5	2.1		100	10*	0.01	79.93	322	3.22	50
	Enceladus	0.1	5.3		50	5	0.005	0.12	32	0.63	15
Simulations											
	Europa	3.0	1.0	40	40	100	0.1	959	1046	26.16	35
	Saline Enceladus	0.1	5.3	10	40	100	0.1	2.45	67	1.68	35
	Fresh Enceladus	0.1	5.3	10	40	100	0.1	2.45	67	1.68	15

262 lateral dilution. Following Speer and Marshall (1995) and Helfrich (1994), the influence  
 263 of rotation on the buoyant plume can be expressed in terms of an appropriately defined  
 264 natural Rossby number:

$$Ro^* = \frac{1}{H} \left( \frac{F}{f^3} \right)^{1/4}, \quad (4)$$

265 where

$$F = \int \int B \, dx \, dy \quad (5)$$

266 is the magnitude of the buoyancy flux integrated over the area of the heating patch with  
 267 units of ( $m^4s^{-3}$ ),  $f = 2\Omega$  is the rotation rate of the system, and  $H$  is the depth of the  
 268 fluid — see (Jones & Marshall, 1993; Maxworthy & Narimousa, 1994; Goodman & Lenferink,  
 269 2012). The length scale

$$l_{rot} = \left( \frac{F}{f^3} \right)^{1/4} \quad (6)$$

270 is a measure of the distance a buoyant parcel of fluid travels in a rotation period. Thus,  
 271 the natural Rossby number can essentially be thought of as a ratio of two length scales,  
 272  $l_{rot}$  and  $H$ ; if the ratio is small the depth of the ocean is much larger than the distance  
 273 traveled by a heated parcel in one day, while if the ratio is large the parcel reaches the  
 274 surface at height  $H$  before rotation can influence its motion. As discussed in Bire et al  
 275 (2022),  $Ro^*$  has great utility because it only depends on externally-prescribed param-  
 276 eters which are somewhat constrained by observations and is independent of uncertain  
 277 eddy viscosities and diffusivities which are set by the nature of unresolved and unobserv-  
 278 able small-scale turbulence.

279 Table 1 sets out the values of key dimensional and non-dimensional parameters for  
 280 hydrothermal activity on Enceladus and Europa, together with those same parameters  
 281 for the numerical experiments presented here. Note that Enceladus, due to its small gravi-  
 282 ty and tiny thermal expansion coefficient, typically has very weak buoyancy forcing,  $F$ ,  
 283 (even after prescribing an order-of-magnitude more localization than suggested by Choblet  
 284 et al. (2017)) and a very small value of  $Ro^*$ , roughly commensurate with the  $Ro^*$  per-  
 285 taining to the experiment shown in Fig. 3. This should be contrasted with Europa which,  
 286 due its larger gravity and larger expansion coefficient, has an  $F$  which is almost three  
 287 orders of magnitude larger. Europa is also thought to be a considerably deeper ocean  
 288 than Enceladus. These two factors lead to an  $Ro^*$  on Europa which is 5 times larger than  
 289 that on Enceladus, although it remains much smaller than unity.

290 In the studies of Goodman and Lenferink (2012), a highly concentrated heat, and  
 291 thus buoyancy flux, for Europa led to plumes reaching all the way up to the surface within  
 292 15 – 20 days even after inhibition by rotation. For the purpose of cross comparison, we  
 293 reproduce one of their calculations in Fig.4 which illustrates the response to larger buoy-  
 294 ancy fluxes appropriate to Europa. Note that for the parameters assumed in Fig.4 (which  
 295 are from one of the experiments in Goodman and Lenferink (2012)), representative of  
 296 a high heat flux end-member for Europa,  $F$  is more than 100 times larger than is per-  
 297 haps reasonable, and  $Ro^*$  order 10 times larger. In this case a plume rising from (and  
 298 particles released from) a hydrothermal vent at the bottom travels all the way to the sur-  
 299 face in several 10s of days. It is perhaps not implausible that some of the icy surface ge-  
 300 omorphology seen on Europa could be evidence of hydrothermal activity from below.

301 But what happens if we assume that the water making up our ocean is very fresh  
 302 rather than salty, with a negative expansion coefficient?

## 303 5 Bottom spreading gravity currents in fresh oceans

304 Fig. 5 shows typical flow patterns of plumes heated in a fresh ocean in which the  
 305 salinity is set to 15 psu, near freezing temperatures. For icy moons like Enceladus, the



306 water is expected to be close to freezing temperatures which means that the coefficient  
 307 of thermal expansion becomes negative. Thus, the water directly above the heating patch  
 308 initially becomes warm and dense. Continuous heating from the warm patch provides  
 309 an uninterrupted supply of dense water. As a result, the dense water initially spreads  
 310 radially outwards along the bottom. A short while later, it comes under the influence  
 311 of rotation and forms an anticyclonic circulation around the source (heating patch) as  
 312 can be seen in Fig. 5d. Eventually, as more and more dense water is supplied from the  
 313 patch, the outflow forms four secondary vortices (panels e, g, i). The temperature sig-  
 314 nature and the particles released at the bottom shown in panels c and k, respectively,  
 315 further show that the plume does not become buoyant at least in the first 400 rotation  
 316 periods.

317 Literature on continuously forced gravity currents is sparse but there is some liter-  
 318 ature on lock release experiments which is relevant to the present study (e.g. Saun-  
 319 ders, 1973; Griffiths & Linden, 1981; Dai & Wu, 2016, 2018). Typically, they involve re-  
 320 leasing a fluid of high or low density into another fluid of a background density in a ro-  
 321 tating system. If a dense fluid is released into a fluid of low background density, it nat-  
 322 urally settles at the bottom, while if the released fluid is light, it rises to the top. In the  
 323 former case, the dense fluid has some effects due to bottom friction but the two cases  
 324 are rather similar to one-another (Saunders, 1973). Such experiments allow us to study  
 325 how these fluids of distinct densities transition to a stable state.

326 The difference in density provides a parameter known as the reduced gravity or buoy-  
 327 ancy given by

$$g' = g \frac{\rho_1 - \rho_0}{\rho_0} = -b, \quad (7)$$

328 where  $g$  is the acceleration due to gravity and  $\rho_0$  is the density of the background fluid  
 329 and  $\rho_1$  is that of the released fluid. Another crucial parameter is the volume of dense  
 330 fluid released which is measured in terms of the radius of the cylinder,  $R$ , and its height,  
 331  $h$ . Most studies tend to use a cylindrical lock extending across the water column,  $H$ , which  
 332 allows them to characterize the volume of fluid released in terms of  $R$  only. The Rossby  
 333 radius of deformation,

$$l_\rho = \frac{\sqrt{g'H}}{f}, \quad (8)$$

334 gives a limiting length scale at which the propagating gravity waves are influenced by  
 335 rotation. In the lock release experiments, the ratio of this length scale to that of the ra-  
 336 dius of the cylindrical lock,  $R$ , is proportional to the ratio of inertial to Coriolis terms  
 337 in the momentum equation,

$$B = \frac{l_\rho^2}{R^2}. \quad (9)$$

338 where  $B$  is a Burger number. Depending on the value of  $B$ , the heavy fluid flowing out-  
 339 wards undergoes different dynamics. For low values of  $B$ , the Coriolis forces become im-  
 340 portant and the outflow breaks up into independent vortices, the vortex splitting described  
 341 by Saunders (1973). For intermediate values, vortex wandering occurs in which the flow  
 342 around the lock forms a vortex but it never detaches from the primary vortex and in-  
 343 stead rotates around it. For high values of  $B$ , the Coriolis forces are small and the out-  
 344 flow reaches a maximum radius as the radial flow is diverted in the azimuthal direction  
 345 and forms a bulbs-and-wedges pattern at the outer boundary (Dai & Wu, 2016, 2018).

346 Griffiths and Linden (1981) performed laboratory experiments in which they com-  
 347 pared constant volume lock-release cases with constant flux cases (fluid is released at the  
 348 top at a constant rate). In the constant flow rate case, they find that the light fluid spreads  
 349 at the surface initially for  $\sim 1-2$  rotation periods after which baroclinic instability de-  
 350 velops on the near vertical interface between the light and dense fluid for the case of low  
 351  $B$ . The baroclinic instability is initially small but grows with time and imparts a non-  
 352 axisymmetric nature to the flow. The non-axisymmetric component of the flow eventu-  
 353 ally grows to shed independent vortices from the main initial vortex. The number of new

354 vortices shed again depends on the ratio of Coriolis to buoyancy forces, as well as on the  
 355 depth occupied by the injected flow. This behavior is qualitatively similar to results from  
 356 our experiment in which the Rossby radius of deformation is order 100s of m and much  
 357 smaller than the domain size ( $R$ ), leading to a small value of  $B$  and hence vortex split-  
 358 ting.

359 Although Griffiths and Linden (1981) were able to characterize an empirical rela-  
 360 tionship between the number of secondary vortices and non-dimensional parameters such  
 361 as  $B$  and  $h/H$ , their domain was horizontally constrained and boundary effects became  
 362 significant. In addition, in their experiments, the depth of the injected flow may become  
 363 comparable to the Ekman layer leading to substantial viscous effects. Both Saunders (1973)  
 364 and Griffiths and Linden (1981) find that viscous effects facilitate secondary vortex for-  
 365 mation in surface as well as bottom Ekman layers. Thus, further research needs to be  
 366 undertaken to understand (i) the nature of vortex splitting in the constant flux case and  
 367 (ii) the effect of Ekman layers and bottom friction on flow instability. Nevertheless, our  
 368 results, when combined with existing work on forced gravity currents, suggests that hy-  
 369 drothermal plumes in a fresh ocean are likely to lead to the formation of unstable vor-  
 370 tices of dense fluid near the seafloor. This scenario is very different from the plummy con-  
 371 vection observed on heating a fluid in which the thermal expansion coefficient is posi-  
 372 tive. The choice of 15 psu here is based on TEOS-10 and has been chosen for illustra-  
 373 tive purposes. In the real Enceladean ocean, as long as the salt composition and con-  
 374 centration allows anomalous contraction of water on heating, the bottom spreading case  
 375 is likely to occur.

## 376 6 Discussion — Implications for icy moons

377 Our results highlight the critical role of seawater salinity and ocean depth on con-  
 378 trolling hydrothermal plume dynamics in icy ocean worlds. In particular, we conclude  
 379 that on Europa vents may induce “buoyant” hydrothermal plumes because the ocean is  
 380 perhaps salty and deep, and so the thermal expansion coefficient positive: hydrothermal  
 381 activity reminiscent of that on Earth will likely ensue, as studied for example in Goodman  
 382 and Lenferink (2012). Enceladus, instead, may have “dense” hydrothermal activity due  
 383 to it being fresher and shallower and thus possessing, perhaps, a negative thermal ex-  
 384 pansion coefficient: heavy fluid would then flow out from venting systems hugging the  
 385 bottom. Owing to the resulting stable stratification and a steady supply of minerals from  
 386 the core, the bottom dense layer could become chemically enriched. This mineral-rich  
 387 dense layer and its interface with the lighter layer above, could potentially provide rich  
 388 habitats for chemosynthetic life away from any liquid-solid interface like the base of the  
 389 ice shell or the seafloor. It has long been known that chemosynthetic microbial activ-  
 390 ity can occur at chemical gradients in mid-water away from any liquid-solid interface,  
 391 as described at redox interfaces in anoxic basins such as the Black Sea and Saanich In-  
 392 let since the 1980s (Tebo et al., 1984). The same processes are now recognized to also  
 393 be present across large swathes of Earth’s deep ocean basins within oxygen minimum  
 394 zones, for example across much of the Eastern Tropical Pacific Ocean and across the Ara-  
 395 bian Sea in northern Indian Ocean where a diversity of microbial metabolic niches are  
 396 sustained. Since the Enceladus’ rocky core likely has high porosity (Choblet et al., 2017),  
 397 the dense hydrothermal fluid could also strongly affect the shallow porous flow in the  
 398 core by enhancing fluid flow into the core. This could provide an additional mechanism  
 399 to stimulate chemically-fuelled microbial activity in a deep sub-seafloor biosphere on Ence-  
 400 lадus — an area of research that is of particular current interest here on Earth (Cario  
 401 et al., 2019).

402 It should be noted that our study has made a number of key simplifications. Our  
 403 simulations were initialized from a state of rest and the background temperature of the  
 404 entire water column is assumed to be at the freezing temperature of water just under  
 405 the ice sheet. If we consider large scale ocean dynamics as well as long term dynamics

406 of hydrothermal plumes, the ambient water into which the hydrothermal plumes inject  
 407 their warm water may be very different on present day Enceladus and Europa than that  
 408 assumed in our study. For example, one could consider a scenario in which Enceladus'  
 409 ocean temperature is initially homogeneous and warm, heavy water, injected from the  
 410 hydrothermal vents spreads along the bottom as suggested by our calculations. This pro-  
 411 cess would lead to a gradual build up of a warm dense layer along the bottom with a light  
 412 layer above it (assuming no flow into the porous rocky core). Over a long period of ge-  
 413 ological time, accumulation of warm water at the bottom would build up so much heat  
 414 in the bottom layer that the thermal expansion coefficient would ultimately become pos-  
 415 itive. This would drive convection in a thick ocean layer overlain by a linearly stratified  
 416 colder water layer under the ice shell (Kang et al., 2022; Zeng & Jansen, 2021). In this  
 417 case, we speculate that the full plume dynamics may behave differently compared to the  
 418 end-members studied in our analysis. Whether the convection would be continuous or  
 419 intermittent should be a topic of further study, taking into account effects of the large  
 420 scale ocean circulation.

## 421 7 Conclusions

422 For terrestrial seawater with salinity exceeding  $22 \text{ g kg}^{-1}$ , water heated by the hy-  
 423 drothermal vents becomes buoyant and rises. However, as argued recently by Kang et  
 424 al. (2022), Enceladus may have an ocean which is fresher than that on earth, in line with  
 425 the chemical equilibrium state obtained from consideration of the Enceladus' water-rock  
 426 ratio in laboratory experiments (Zolotov, 2007; Zolotov & Postberg, 2014; Glein et al.,  
 427 2018a). As shown in fig. 1a,c, and e, the value of  $\alpha$  can be negative for a wide range of  
 428 depths if the temperature is between  $-2$  to  $2^\circ\text{C}$ . In such a case, gravity currents spread-  
 429 ing along the sea floor is a more likely scenario on Enceladus than plumes reaching all  
 430 the way to the surface.

431 In contrast, in the case of Europa, the ocean is expected to be more saline or have  
 432 dissolved components which increase the thermal expansion coefficient of seawater. Ad-  
 433 ditionally, its gravity is stronger and so buoyancy fluxes large, suggesting that plumes  
 434 might reach all the way to the ice shell. Even if Europa turns out to be fresh, the depth  
 435 of Europa's ocean and its higher gravity means that pressure effects would be a more  
 436 prominent factor in setting the thermodynamic equation of state rather than temper-  
 437 ature and salinity. Fig. 1a shows that negative values of  $\alpha$  can only be achieved at ex-  
 438 tremely low salinities ( $< 5$  psu) and shallow depths ( $\sim 5$  km). Thus, even if Europa's  
 439 ocean is fresh, we expect that plumes of buoyant fluid could indeed rise to the surface  
 440 as postulated in Goodman et al. (2004); Goodman and Lenferink (2012).

441 Overall, this study uncovers a fundamental distinction in hydrothermal plume be-  
 442 havior based on the salinity of ambient water. This distinction becomes especially im-  
 443 portant for Enceladus but may not be substantial for Europa. Further, these results could  
 444 potentially influence the decision-making process on choosing an icy moon to visit, at  
 445 least in the short term. On a moon like Europa, which is likely to have more vigorous  
 446 convection and more efficient seafloor to ice-shell transport which leaves its imprint on  
 447 the ice shell. Thus, if the primary icy-ocean world habitable interface is the seafloor, it  
 448 may be a more appealing prospect to focus on Europa than Enceladus because our cur-  
 449 rent technological limitations make ice shells much more accessible than deep ocean. On  
 450 the other hand, Enceladus's deep ocean could be stratified potentially providing chem-  
 451 ical gradients for chemosynthetic life to thrive even within the ocean instead of just the  
 452 seafloor.

## 453 Acknowledgments

454 This work was carried out in the Department of Earth, Atmospheric and Planetary Sci-  
 455 ence (EAPS) in MIT. TM, WK acknowledges endowed funds in EAPS. JM and SB ac-

456 knowledges part-support from NASA Astrobiology Grant 80NSSC19K1427 “Exploring  
457 Ocean Worlds”. We all thank “Exploring Ocean Worlds” for helpful support and discus-  
458 sions.

459 Oceananigans.jl (Ramadhan et al., 2020) was used to perform numerical simula-  
460 tions used in this study. Data from the numerical simulations and analysis code used  
461 in this study is available at Bire (2023).

## 462 References

- 463 Ashkenazy, Y., & Tziperman, E. (2021, Nov). Dynamic Europa ocean shows tran-  
464 sient Taylor columns and convection driven by ice melting and salinity. *Nat.*  
465 *Commun.*, 12(1). Retrieved from [http://dx.doi.org/10.1038/s41467-021-](http://dx.doi.org/10.1038/s41467-021-26710-0)  
466 [26710-0](http://dx.doi.org/10.1038/s41467-021-26710-0) doi: 10.1038/s41467-021-26710-0
- 467 Beuthe, M., Rivoldini, A., & Trinh, A. (2016, Oct). Enceladus’s and Dione’s floating  
468 ice shells supported by minimum stress isostasy. *Geophys. Res. Lett.*, 43(19),  
469 10,088–10,096. Retrieved from <http://dx.doi.org/10.1002/2016GL070650>  
470 doi: 10.1002/2016gl070650
- 471 Bire, S. (2023). *Juicy moons plumes*. Zenodo. Retrieved from [https://zenodo.org/](https://zenodo.org/record/7502389)  
472 [record/7502389](https://zenodo.org/record/7502389) doi: 10.5281/ZENODO.7502389
- 473 Bire, S., Kang, W., Ramadhan, A., Campin, J., & Marshall, J. (2022, Mar). Explor-  
474 ing ocean circulation on icy moons heated from below. *J. Geophys. Res. Plan-*  
475 *ets*, 127(3). Retrieved from <http://dx.doi.org/10.1029/2021JE007025> doi:  
476 10.1029/2021je007025
- 477 Běhouňková, M., Tobie, G., Choblet, G., Kervazo, M., Melwani Daswani, M.,  
478 Dumoulin, C., & Vance, S. D. (2021, Feb). Tidally induced magmatic  
479 pulses on the oceanic floor of Jupiter’s moon Europa. *Geophys. Res. Lett.*,  
480 48(3). Retrieved from <http://dx.doi.org/10.1029/2020GL090077> doi:  
481 10.1029/2020gl090077
- 482 Cable, M. L., Porco, C., Glein, C. R., German, C. R., MacKenzie, S. M., Neveu, M.,  
483 ... Núñez, J. (2021, Jul). The science case for a return to Enceladus. *Planet.*  
484 *Sci. J.*, 2(4), 132. Retrieved from <http://dx.doi.org/10.3847/PSJ/abfb7a>  
485 doi: 10.3847/psj/abfb7a
- 486 Čadek, O., Souček, O., & Běhouňková, M. (2019, Dec). Is Airy isostasy applicable to  
487 icy moons? *Geophys. Res. Lett.*, 46(24), 14299–14306. Retrieved from [http://](http://dx.doi.org/10.1029/2019GL085903)  
488 [dx.doi.org/10.1029/2019GL085903](http://dx.doi.org/10.1029/2019GL085903) doi: 10.1029/2019gl085903
- 489 Čadek, O., Tobie, G., Van Hoolst, T., Massé, M., Choblet, G., Lefèvre, A., ... Trinh,  
490 A. (2016, Jun). Enceladus’s internal ocean and ice shell constrained from  
491 cassini gravity, shape, and libration data. *Geophys. Res. Lett.*, 43(11), 5653–  
492 5660. Retrieved from <http://dx.doi.org/10.1002/2016GL068634> doi:  
493 10.1002/2016gl068634
- 494 Cario, A., Oliver, G. C., & Rogers, K. L. (2019, Sep). Exploring the deep marine  
495 biosphere: Challenges, innovations, and opportunities. *Front. Earth Sci.*,  
496 7. Retrieved from <http://dx.doi.org/10.3389/feart.2019.00225> doi:  
497 10.3389/feart.2019.00225
- 498 Choblet, G., Tobie, G., Buch, A., Čadek, O., Barge, L. M., Běhouňková, M., ...  
499 Van Hoolst, T. (2021, Nov). Enceladus as a potential oasis for life: Sci-  
500 ence goals and investigations for future explorations. *Exp. Astron.* Re-  
501 trieved from <http://dx.doi.org/10.1007/s10686-021-09808-7> doi:  
502 10.1007/s10686-021-09808-7
- 503 Choblet, G., Tobie, G., Sotin, C., Běhouňková, M., Čadek, O., Postberg, F., &  
504 Souček, O. (2017, Nov). Powering prolonged hydrothermal activity inside  
505 Enceladus. *Nat. Astron.*, 1(12), 841–847. Retrieved from [http://dx.doi.org/](http://dx.doi.org/10.1038/s41550-017-0289-8)  
506 [10.1038/s41550-017-0289-8](http://dx.doi.org/10.1038/s41550-017-0289-8) doi: 10.1038/s41550-017-0289-8
- 507 Dai, A., & Wu, C.-S. (2016, Sep). High-resolution simulations of cylindrical grav-

- ity currents in a rotating system. *J. Fluid Mech.*, 806, 71–101. Retrieved from <http://dx.doi.org/10.1017/jfm.2016.598> doi: 10.1017/jfm.2016.598
- Dai, A., & Wu, C.-S. (2018, Feb). High-resolution simulations of unstable cylindrical gravity currents undergoing wandering and splitting motions in a rotating system. *Phys. Fluids*, 30(2), 026601. Retrieved from <http://dx.doi.org/10.1063/1.5011070> doi: 10.1063/1.5011070
- Ede, A. J. (1956, Nov). The influence of anomalous expansion on natural convection in water. *Appl. Sci. Res.*, 5(6), 458–460. Retrieved from <http://dx.doi.org/10.1007/BF03184607> doi: 10.1007/bf03184607
- Fifer, L. M., Catling, D. C., & Toner, J. D. (2022, Aug). Chemical fractionation modeling of plumes indicates a gas-rich, moderately alkaline Enceladus ocean. *Planet. Sci. J.*, 3(8), 191. Retrieved from <http://dx.doi.org/10.3847/PSJ/ac7a9f> doi: 10.3847/psj/ac7a9f
- Fox-Powell, M. G., & Cousins, C. R. (2021). Partitioning of crystalline and amorphous phases during freezing of simulated enceladus ocean fluids. *Journal of Geophysical Research: Planets*, 126(1), e2020JE006628.
- Glass, J., Dierssen, H., Glein, C., Schmidt, B., & Winebrenner, D. (2022). Defining and characterizing habitable environments in ocean world systems. *Oceanography*. Retrieved from <http://dx.doi.org/10.5670/oceanog.2021.414> doi: 10.5670/oceanog.2021.414
- Glein, C., Postberg, F., & Vance, S. (2018a). The geochemistry of enceladus: Composition and controls. *Enceladus and the icy moons of Saturn*, 39.
- Glein, C., Postberg, F., & Vance, S. D. (2018b, Jan). The geochemistry of Enceladus: Composition and controls. In (chap. 3). The University of Arizona Press. Retrieved from [http://dx.doi.org/10.2458/azu\\_uapress\\_9780816537075-ch003](http://dx.doi.org/10.2458/azu_uapress_9780816537075-ch003) doi: 10.2458/azu\_uapress\_9780816537075-ch003
- Goodman, J. C., Collins, G. C., Marshall, J., & Pierrehumbert, R. T. (2004). Hydrothermal plume dynamics on Europa: Implications for chaos formation. *J. Geophys. Res.*, 109(E3). Retrieved from <http://dx.doi.org/10.1029/2003JE002073> doi: 10.1029/2003je002073
- Goodman, J. C., & Lenferink, E. (2012, Nov). Numerical simulations of marine hydrothermal plumes for Europa and other icy worlds. *Icarus*, 221(2), 970–983. Retrieved from <http://dx.doi.org/10.1016/j.icarus.2012.08.027> doi: 10.1016/j.icarus.2012.08.027
- Griffiths, R. W., & Linden, P. F. (1981, Apr). The stability of vortices in a rotating, stratified fluid. *J. Fluid Mech.*, 105(-1), 283. Retrieved from <http://dx.doi.org/10.1017/S0022112081003212> doi: 10.1017/s0022112081003212
- Hand, K., & Chyba, C. (2007, August). Empirical constraints on the salinity of the european ocean and implications for a thin ice shell. *Icarus*, 189(2), 424–438.
- Hand, K., Sotin, C., Hayes, A., & Coustenis, A. (2020, Jul). On the habitability and future exploration of ocean worlds. *Space Sci. Rev.*, 216(5). Retrieved from <http://dx.doi.org/10.1007/s11214-020-00713-7> doi: 10.1007/s11214-020-00713-7
- Hansen, C. J., Esposito, L., Stewart, A. I. F., Colwell, J., Hendrix, A., Pryor, W., ... West, R. (2006, Mar). Enceladus’ water vapor plume. *Science*, 311(5766), 1422–1425. Retrieved from <http://dx.doi.org/10.1126/science.1121254> doi: 10.1126/science.1121254
- Helfrich, K. R. (1994, Jan). Thermals with background rotation and stratification. *J. Fluid Mech.*, 259, 265–280. Retrieved from <http://dx.doi.org/10.1017/S0022112094000121> doi: 10.1017/s0022112094000121
- Hemingway, D. J., & Mittal, T. (2019, Nov). Enceladus’s ice shell structure as a window on internal heat production. *Icarus*, 332, 111–131. Retrieved from <http://dx.doi.org/10.1016/j.icarus.2019.03.011> doi: 10.1016/j.icarus.2019.03.011
- Hsu, H.-W., Postberg, F., Sekine, Y., Shibuya, T., Kempf, S., Horányi, M., ... Srama,

- 563 R. (2015, Mar). Ongoing hydrothermal activities within Enceladus. *Nature*, 519(7542), 207–210. Retrieved from <http://dx.doi.org/10.1038/nature14262> doi: 10.1038/nature14262
- 564  
565
- 566 Ingersoll, A. P., & Nakajima, M. (2016). Controlled boiling on enceladus. 2. model  
567 of the liquid-filled cracks. *Icarus*, 272, 319–326.
- 568 Ivanov, D., & Nikolov, S. (2020, Jul). The anomalous thermal expansion of water.  
569 *Phys. Educ.*, 55(5), 055008. Retrieved from <http://dx.doi.org/10.1088/1361-6552/ab9480>  
570 doi: 10.1088/1361-6552/ab9480
- 571 Jones, H., & Marshall, J. (1993, Jun). Convection with rotation in a neutral ocean:  
572 A study of open-ocean deep convection. *J. Phys. Oceanogr.*, 23(6), 1009–1039.  
573 Retrieved from [http://dx.doi.org/10.1175/1520-0485\(1993\)023<1009:CWRIAN>2.0.CO;2](http://dx.doi.org/10.1175/1520-0485(1993)023<1009:CWRIAN>2.0.CO;2)  
574 doi: 10.1175/1520-0485(1993)023<1009:cwrian>2.0.co;2
- 575 Kang, W., Mittal, T., Bire, S., Campin, J.-M., & Marshall, J. (2022, Jul). How does  
576 salinity shape ocean circulation and ice geometry on Enceladus and other icy  
577 satellites? *Sci. Adv.*, 8(29). Retrieved from <http://dx.doi.org/10.1126/sciadv.abm4665>  
578 doi: 10.1126/sciadv.abm4665
- 579 Khawaja, N., Postberg, F., Hillier, J., Klenner, F., Kempf, S., Nölle, L., ... Srama,  
580 R. (2019, Oct). Low-mass nitrogen-, oxygen-bearing, and aromatic compounds  
581 in Enceladean ice grains. *Monthly Notices of the Royal Astronomical Society*,  
582 489(4), 5231–5243. Retrieved from <http://dx.doi.org/10.1093/mnras/stz2280>  
583 doi: 10.1093/mnras/stz2280
- 584 Kvoraka, J., Čadek, O., Tobie, G., & Choblet, G. (2018, Aug). Does Titan’s long-  
585 wavelength topography contain information about subsurface ocean dynam-  
586 ics? *Icarus*, 310, 149–164. Retrieved from <http://dx.doi.org/10.1016/j.icarus.2017.12.010>  
587 doi: 10.1016/j.icarus.2017.12.010
- 588 MacKenzie, S. M., Neveu, M., Davila, A. F., Lunine, J. I., Cable, M. L., Phillips-  
589 Lander, C. M., ... Heldmann, J. (2022, Jun). Science objectives for flagship-  
590 class mission concepts for the search for evidence of life at Enceladus. *As-  
591 trobiology*, 22(6), 685–712. Retrieved from <http://dx.doi.org/10.1089/ast.2020.2425>  
592 doi: 10.1089/ast.2020.2425
- 593 Maxworthy, T., & Narimousa, S. (1994, May). Unsteady, turbulent con-  
594 vection into a homogeneous, rotating fluid, with oceanographic applica-  
595 tions. *J. Phys. Oceanogr.*, 24(5), 865–887. Retrieved from [http://dx.doi.org/10.1175/1520-0485\(1994\)024<0865:UTCIAH>2.0.CO;2](http://dx.doi.org/10.1175/1520-0485(1994)024<0865:UTCIAH>2.0.CO;2) doi:  
596 10.1175/1520-0485(1994)024<0865:utciah>2.0.co;2
- 597
- 598 Millero, F. J., Feistel, R., Wright, D. G., & McDougall, T. J. (2008, Jan). The com-  
599 position of standard seawater and the definition of the reference-composition  
600 salinity scale. *Deep Sea Res. Part I Oceanogr. Res. Pap.*, 55(1), 50–72.  
601 Retrieved from <http://dx.doi.org/10.1016/j.dsr.2007.10.001> doi:  
602 10.1016/j.dsr.2007.10.001
- 603 Nimmo, F., & Pappalardo, R. T. (2016, Aug). Ocean worlds in the outer solar sys-  
604 tem. *J. Geophys. Res. Planets*, 121(8), 1378–1399. Retrieved from <http://dx.doi.org/10.1002/2016JE005081> doi: 10.1002/2016je005081
- 605
- 606 Porco, C. C., Helfenstein, P., Thomas, P. C., Ingersoll, A. P., Wisdom, J., West, R.,  
607 ... Squyres, S. (2006, Mar). Cassini observes the active south pole of Enceladus.  
608 *Science*, 311(5766), 1393–1401. Retrieved from <http://dx.doi.org/10.1126/science.1123013>  
609 doi: 10.1126/science.1123013
- 610 Postberg, F., Kempf, S., Schmidt, J., Brilliantov, N., Beinsen, A., Abel, B., ...  
611 Srama, R. (2009). Sodium salts in e-ring ice grains from an ocean below  
612 the surface of enceladus. *Nature*, 459(7250), 1098–1101.
- 613 Postberg, F., Khawaja, N., Abel, B., Choblet, G., Glein, C. R., Gudipati, M. S.,  
614 ... Waite, J. H. (2018, Jun). Macromolecular organic compounds from the  
615 depths of Enceladus. *Nature*, 558(7711), 564–568. Retrieved from <http://dx.doi.org/10.1038/s41586-018-0246-4>  
616 doi: 10.1038/s41586-018-0246-4
- 617 Postberg, F., Klenner, F., Zou, Z., Hillier, J. K., Khawaja, N., Nölle, L., & Schmidt,

- 618 J. (2022, Sep). Detection of phosphates originating from Enceladus'  
619 ocean by Cassini's cosmic dust analyzer. *Europa Science Congress*  
620 *2022, Granada, Spain, 18–23 Sep 2022, EPSC2022-639*. Retrieved from  
621 <http://dx.doi.org/10.5194/epsc2022-639> doi: 10.5194/epsc2022-639
- 622 Ramadhan, A., Wagner, G., Hill, C., Campin, J.-M., Churavy, V., Besard, T., ...  
623 Marshall, J. (2020, Sep). Oceananigans.jl: Fast and friendly geophysical  
624 fluid dynamics on GPUs. *J. Open Source Softw.*, *5*(53), 2018. Retrieved from  
625 <http://dx.doi.org/10.21105/joss.02018> doi: 10.21105/joss.02018
- 626 Roquet, F., Madec, G., Brodeau, L., & Nycander, J. (2015, Oct). Defining a simpli-  
627 fied yet “realistic” equation of state for seawater. *J. Phys. Oceanogr.*, *45*(10),  
628 2564–2579. Retrieved from <http://dx.doi.org/10.1175/JPO-D-15-0080.1>  
629 doi: 10.1175/jpo-d-15-0080.1
- 630 Rovira-Navarro, M., Katz, R. F., Liao, Y., van der Wal, W., & Nimmo, F. (2022,  
631 May). The tides of Enceladus' porous core. *J. Geophys. Res. Planets*,  
632 *127*(5). Retrieved from <http://dx.doi.org/10.1029/2021JE007117> doi:  
633 10.1029/2021je007117
- 634 Saunders, P. M. (1973, Jan). The instability of a baroclinic vortex. *J. Phys.*  
635 *Oceanogr.*, *3*(1), 61–65. Retrieved from [http://dx.doi.org/10.1175/  
636 1520-0485\(1973\)003<0061:TIOABV>2.0.CO;2](http://dx.doi.org/10.1175/1520-0485(1973)003<0061:TIOABV>2.0.CO;2) doi: 10.1175/1520-0485(1973)  
637 003<0061:tioabv>2.0.co;2
- 638 Sekine, Y., Shibuya, T., Postberg, F., Hsu, H.-W., Suzuki, K., Masaki, Y., ... Sirono,  
639 S.-i. (2015, Oct). High-temperature water–rock interactions and hydrother-  
640 mal environments in the chondrite-like core of Enceladus. *Nat. Commun.*,  
641 *6*(1). Retrieved from <http://dx.doi.org/10.1038/ncomms9604> doi:  
642 10.1038/ncomms9604
- 643 Soderlund, K. M. (2019, Aug). Ocean dynamics of outer solar system satellites.  
644 *Geophys. Res. Lett.*, *46*(15), 8700–8710. Retrieved from [http://dx.doi.org/  
645 10.1029/2018GL081880](http://dx.doi.org/10.1029/2018GL081880) doi: 10.1029/2018gl081880
- 646 Soderlund, K. M., Schmidt, B. E., Wicht, J., & Blankenship, D. D. (2013, Dec).  
647 Ocean-driven heating of Europa's icy shell at low latitudes. *Nat. Geosci.*,  
648 *7*(1), 16–19. Retrieved from <http://dx.doi.org/10.1038/NGE02021> doi:  
649 10.1038/ngeo2021
- 650 Speer, K. G., & Marshall, J. (1995, Nov). The growth of convective plumes at  
651 seafloor hot springs. *J. Mar. Res.*, *53*(6), 1025–1057. Retrieved from [http://  
652 dx.doi.org/10.1357/0022240953212972](http://dx.doi.org/10.1357/0022240953212972) doi: 10.1357/0022240953212972
- 653 Steel, E. L., Davila, A., & McKay, C. P. (2017, Sep). Abiotic and biotic forma-  
654 tion of amino acids in the Enceladus ocean. *Astrobiology*, *17*(9), 862–875. Re-  
655 trieved from <http://dx.doi.org/10.1089/ast.2017.1673> doi: 10.1089/ast  
656 .2017.1673
- 657 Tebo, B. M., Nealson, K. H., Emerson, S., & Jacobs, L. (1984, Nov). Micro-  
658 bial mediation of Mn(II) and Co(II) precipitation at the O<sub>2</sub>/H<sub>2</sub>S inter-  
659 faces in two anoxic fjords. *Limnol. Oceanogr.*, *29*(6), 1247–1258. Re-  
660 trieved from <http://dx.doi.org/10.4319/lo.1984.29.6.1247> doi:  
661 10.4319/lo.1984.29.6.1247
- 662 Thomas, P., Tajeddine, R., Tiscareno, M., Burns, J., Joseph, J., Loredó, T.,  
663 ... Porco, C. (2016, Jan). Enceladus's measured physical libration re-  
664 quires a global subsurface ocean. *Icarus*, *264*, 37–47. Retrieved from  
665 <http://dx.doi.org/10.1016/j.icarus.2015.08.037> doi: 10.1016/  
666 j.icarus.2015.08.037
- 667 Trumbo, S. K., Brown, M. E., & Hand, K. P. (2019, Jun). Sodium chloride on the  
668 surface of Europa. *Sci. Adv.*, *5*(6), eaaw7123. Retrieved from [http://dx.doi  
669 .org/10.1126/sciadv.aaw7123](http://dx.doi.org/10.1126/sciadv.aaw7123) doi: 10.1126/sciadv.aaw7123
- 670 Vance, S., Bouffard, M., Choukroun, M., & Sotin, C. (2014, Jun). Ganymede s in-  
671 ternal structure including thermodynamics of magnesium sulfate oceans in con-  
672 tact with ice. *Planetary and Space Science*, *96*, 62–70. Retrieved from <http://>

- 673 dx.doi.org/10.1016/j.pss.2014.03.011 doi: 10.1016/j.pss.2014.03.011  
 674 Vance, S., Panning, M. P., Stähler, S., Cammarano, F., Bills, B. G., Tobie, G.,  
 675 ... Banerdt, B. (2018, Jan). Geophysical investigations of habitabil-  
 676 ity in ice-covered ocean worlds. *J. Geophys. Res. Planets*, 123(1), 180–  
 677 205. Retrieved from <http://dx.doi.org/10.1002/2017JE005341> doi:  
 678 10.1002/2017je005341
- 679 Van Hoolst, T., Baland, R.-M., & Trinh, A. (2016, Oct). The diurnal libration and  
 680 interior structure of Enceladus. *Icarus*, 277, 311–318. Retrieved from [http://](http://dx.doi.org/10.1016/j.icarus.2016.05.025)  
 681 [dx.doi.org/10.1016/j.icarus.2016.05.025](http://dx.doi.org/10.1016/j.icarus.2016.05.025) doi: 10.1016/j.icarus.2016.05  
 682 .025
- 683 Waite, J. H., Glein, C. R., Perryman, R. S., Teolis, B. D., Magee, B. A., Miller,  
 684 G., ... Bolton, S. J. (2017, Apr). Cassini finds molecular hydrogen in the  
 685 Enceladus plume: Evidence for hydrothermal processes. *Science*, 356(6334),  
 686 155–159. Retrieved from <http://dx.doi.org/10.1126/science.aai8703>  
 687 doi: 10.1126/science.aai8703
- 688 Zeng, Y., & Jansen, M. F. (2021). Ocean circulation on enceladus with a high-versus  
 689 low-salinity ocean. *The Planetary Science Journal*, 2(4), 151.
- 690 Zolotov, M. Y. (2007). An oceanic composition on early and today's enceladus. *Geo-*  
 691 *physical Research Letters*, 34(23).
- 692 Zolotov, M. Y., & Postberg, F. (2014). Can nano-phase silica originate from chon-  
 693 dritic fluids? the application to enceladus' sio2 particles. *LPI(1777)*, 2496.



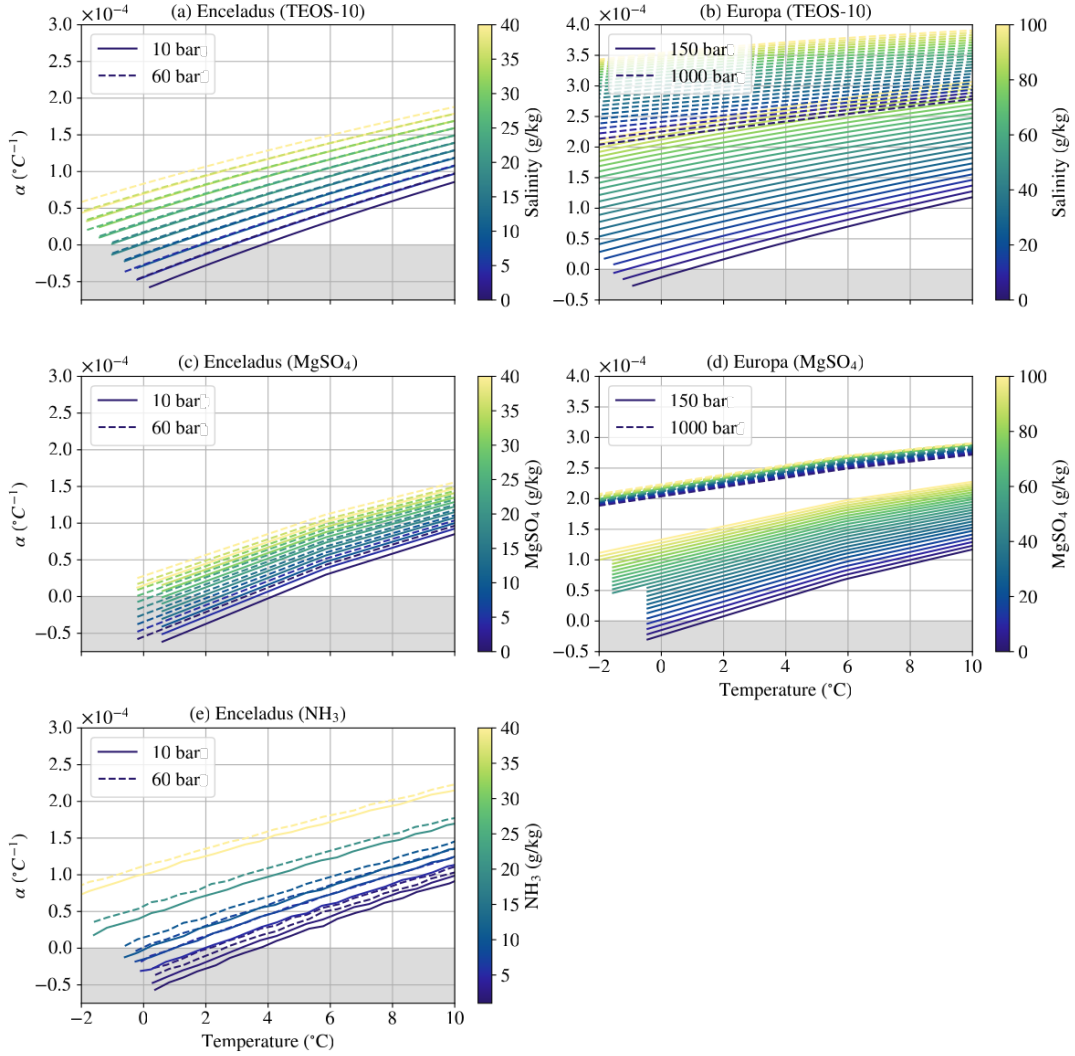


**Figure 1.** The thermal expansion coefficient of (a) seawater, (c) water rich in magnesium sulphate, and (e) water rich in ammonia is shown as a function of temperature (x-axis) and salt concentration (shading). The relationships are plotted for pressures of 10,30, and 60 bar by solid, dashed, and dotted lines, respectively, roughly corresponding to depths of 5, 25, and 50 km on Enceladus. Thermal expansion coefficient of (b) seawater and (d) water rich in magnesium sulphate are shown at pressures of 150, 600, 1000, and 2000 bar, roughly corresponding to depths of 5, 50, 100, and 150 km on Europa. The region shaded in grey picks out parameter values in which the thermal expansion coefficient becomes negative.

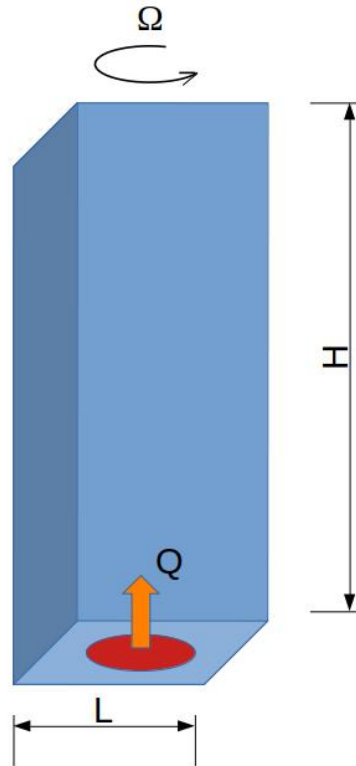


**Figure 2.** The configuration of the numerical model. The domain size is  $10 \times 10 \times 40 \text{ km}^3$ . A heating patch is applied at the bottom with an area of  $1 \times 1 \text{ km}^2$  shown in red which acts as the source of the hydrothermal plume. The resolution of the model is 40 m in the horizontal and 80 m in the vertical.

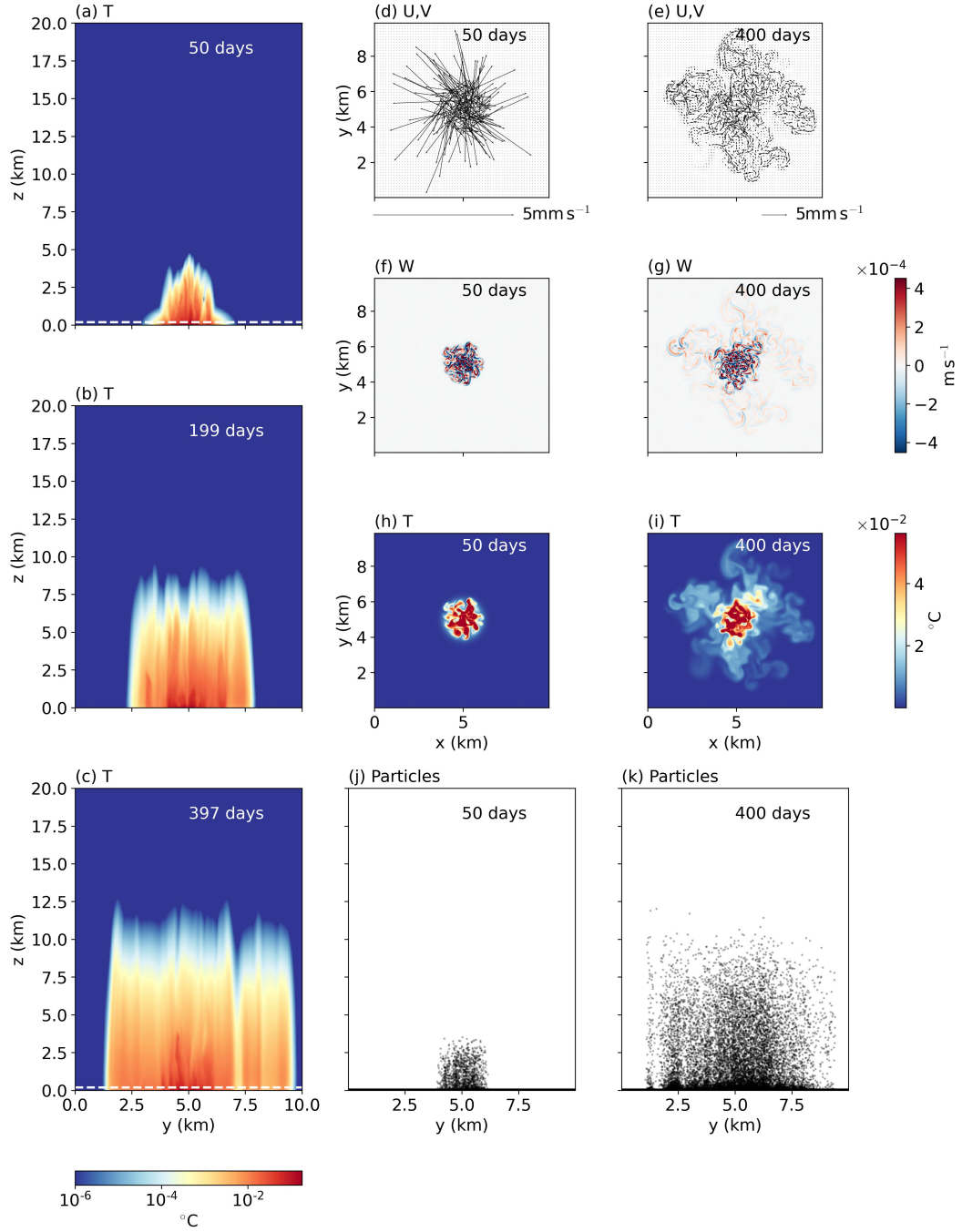


**Figure 3.** Panels a, b, and c show the meridional sections of temperature at  $x = 5$  km due to a hydrothermal plume for a saline ocean at 50, 200, and 400 rotation periods, respectively. Panels d and e show the velocity vectors 80 m above the bottom at 50 and 400 rotation periods, respectively. Panels f and g show the vertical velocity at 50 and 400 rotation periods, respectively. Panels h and i show the plan view of temperature 80 m above the bottom at 50 and 400 rotation periods, respectively. Panels j and k show the meridional sections at  $x = 5$  km of particles initially released at the bottom.

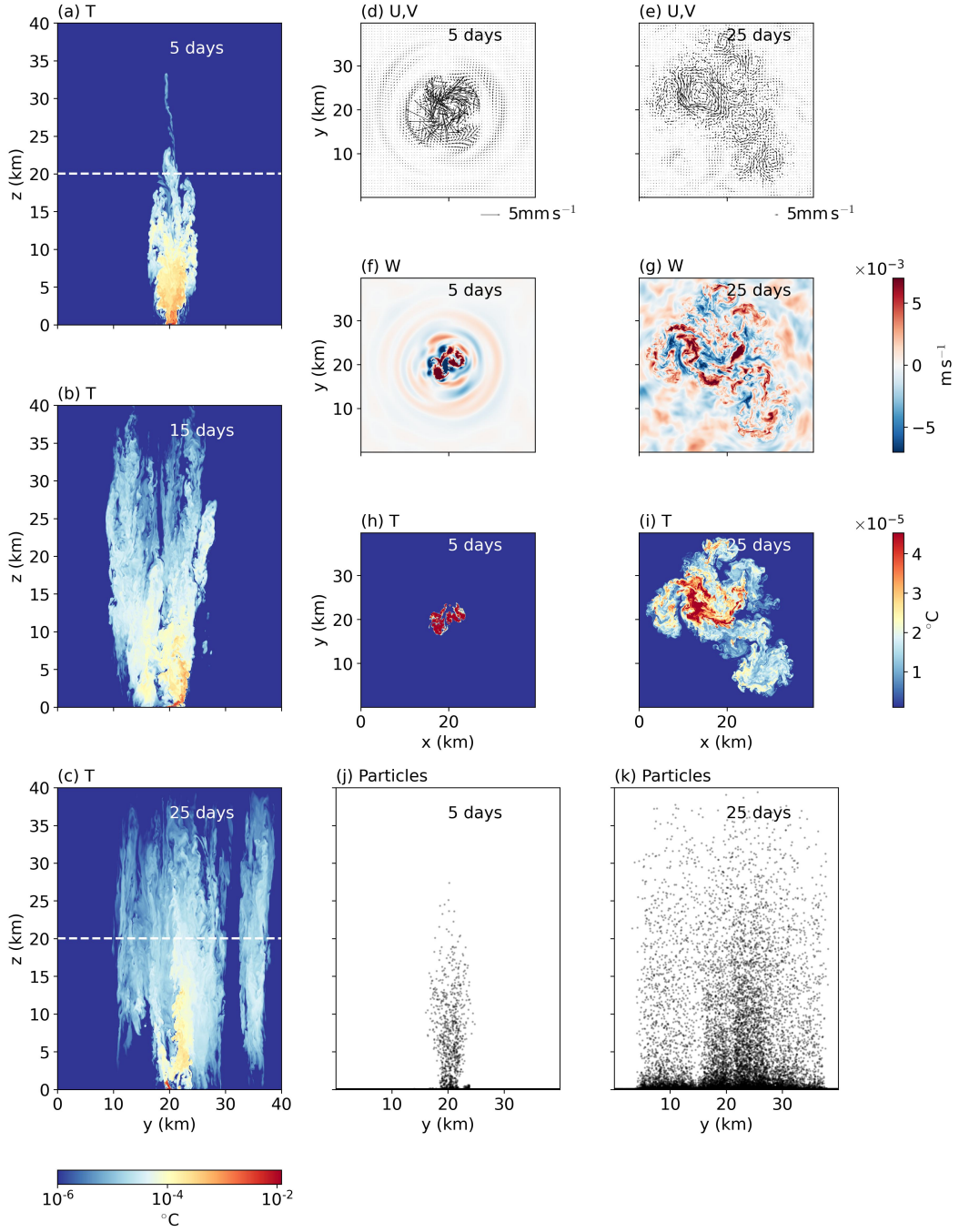


**Figure 4.** Panels a, b, and c show the meridional sections of temperature at  $x = 20$  km due to a hydrothermal plume for a saline ocean at 5, 15, and 25 rotation periods, respectively. Panels d and e show the velocity vectors 20 km above the bottom at 5 and 25 rotation periods, respectively. Panels f and g show the vertical velocity at 5 and 25 rotation periods, respectively. Panels h and i show the plan view of temperature 20 km above the bottom at 5 and 25 rotation periods, respectively. Panels j and k show the meridional sections at  $x = 20$  km of particles initially released at the bottom.

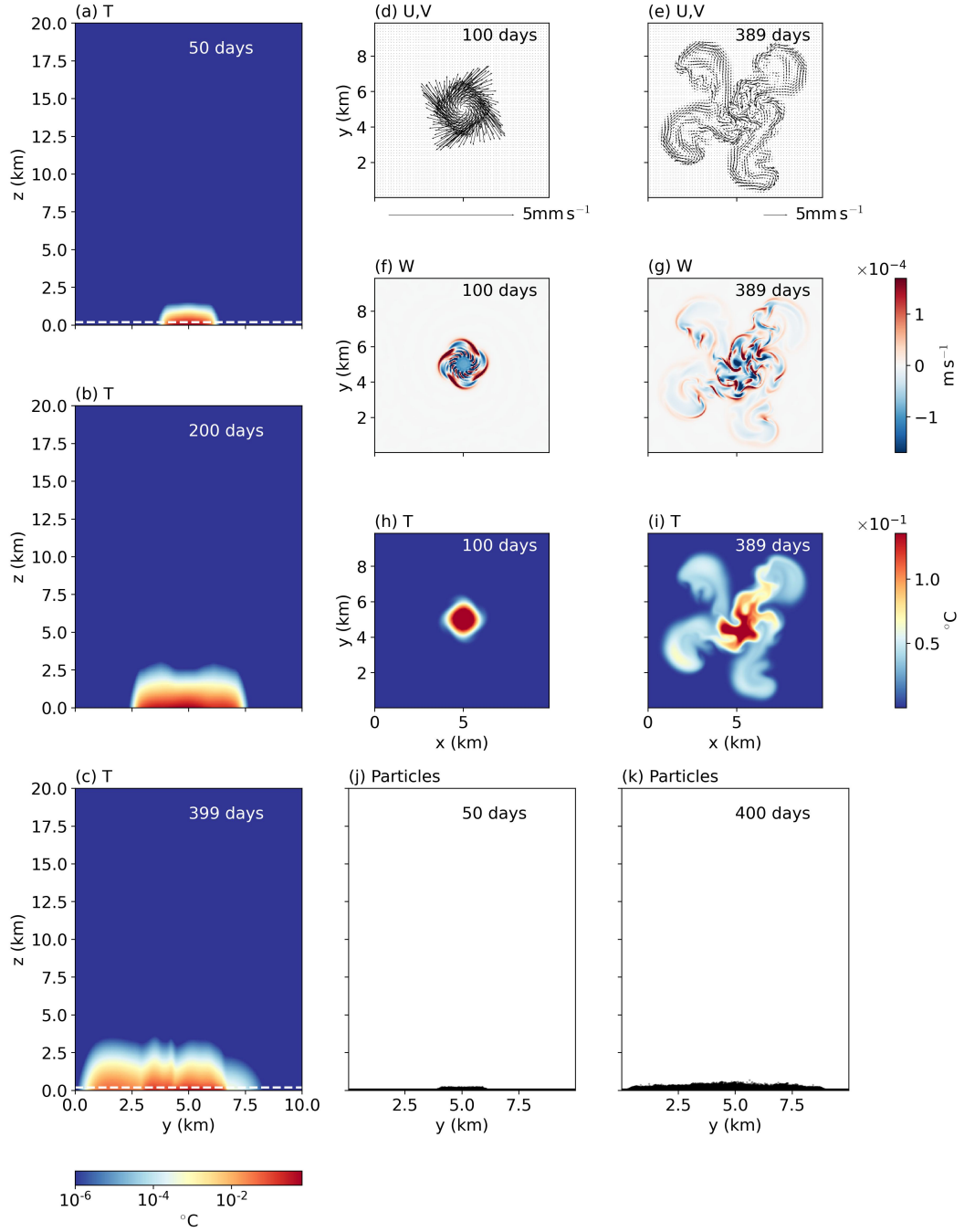


**Figure 5.** Panels a, b, and c show the meridional sections of temperature at  $x = 5$  km due to a hydrothermal plume for a fresh ocean at 50, 200, and 400 rotation periods, respectively. Panels d and e show the velocity vectors 80 m above the bottom at 50 and 400 rotation periods, respectively. Panels f and g show the vertical velocity at 50 and 400 rotation periods, respectively. Panels h and i show the plan view of temperature 80 m above the bottom at 50 and 400 rotation periods, respectively. Panels j and k show the meridional sections at  $x = 5$  km of particles initially released at the bottom.